

Flexural bearing capacity of diaphragm-through joints of concrete-filled square steel tubular columns

Bin Rong¹, Rui Liu¹, Ruoyu Zhang^{*1}, Zhihua Chen² and Fafitis Apostolos³

¹ Department of Civil Engineering, Tianjin University, Tianjin, 300072, China

² Key Laboratory of Coast Civil Structure Safety, Tianjin University, Tianjin, 300072, China

³ Department of Civil and Environmental Engineering, Arizona State University, Tempe, 85287, USA

(Received March 12, 2015, Revised August 14, 2015, Accepted November 04, 2015)

Abstract. In order to investigate the flexural bearing capacity of panel zone of diaphragm-through joint between concrete filled square steel tubular column and steel beam, four specimens were tested under static tension loads to study the mechanical properties and bearing capacity of diaphragm-through joints with a failure mode of panel zone. Finite element models of these specimens were developed to simulate the test and compare the predicted failure modes, load-displacement curves and bearing capacities with the experimentally observed. It was found that the tensile load from the steel beam flange is mainly shared by the square steel tube and the diaphragm. The diaphragm plastic zone appears along the cross-section lines enclosed by the square steel tube and the influence of steel beam web on the plastic zone of the steel tube is significant and cannot be neglected. Computational models of yield lines on square steel tube and diaphragm are established based on the distribution pattern of the plastic zone, and an analytical method for the evaluation of the bearing capacity of the joint is proposed. The theoretical results and the experimental data are compared and found in good agreement.

Keywords: diaphragm-through joint; flexural bearing capacity; static tensile loading experiment; finite element analysis; yield line

1. Introduction

Concrete-filled square steel tubular columns and H-shaped steel beams have gained a widespread usage in composite frame structures. Interior diaphragm joints and diaphragm-through joints which transfer loads from beam to the panel zone of connections by means of diaphragms, shown in Fig. 1, can offer higher bearing capacity and better ductility than joints in which the steel tube is connected to beams without diaphragms (Kim *et al.* 2008, Choi *et al.* 2009, Wang *et al.* 2012, Liu *et al.* 2012 and Tizani *et al.* 2013).

In practical applications, composite frames should be designed as a weak beam- strong column system. However, the reinforced concrete floor slabs attached to the steel beams with shear connectors will cause the flexural capacity of the panel zone of the joints less than that of steel beams with concrete slabs (Han and Li 2010, Zhao *et al.* 2010). Therefore it is necessary to evaluate the flexural capacity of the panel zone of these joints so as to avoid the strong beam-weak column mechanism.

*Corresponding author, Ph.D., E-mail: zryu@163.com

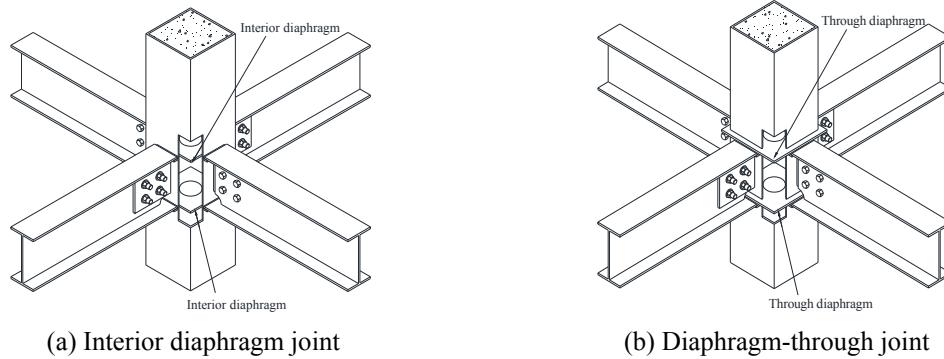


Fig. 1 Joint forms

In the past, some research work has been carried out to investigate the flexural bearing capacity of the panel zone of interior diaphragm joints. Three interior diaphragm joints were tested by Sasaki *et al.* (1995) and five interior diaphragm joints were tested by Lu *et al.* (2000). They found that the flexural bearing capacity of the panel zone should take into account the contribution of the interior diaphragm and the steel tube while the contribution of concrete is small and can be neglected. The yield line theory was employed to evaluate the flexural bearing capacity of the panel zone of interior diaphragm joints. Based on the previous investigations, Nie *et al.* (2008a, b and 2009) tested three interior diaphragm joints and proposed an analytical method considering the axial load effect on the panel zone of interior diaphragm joints.

Given the difference in the configuration of the diaphragm-through and the interior diaphragm joints as depicted in Fig.1, the behavior of these two types of joints are not the same. There are not many studies on the flexural bearing capacity of diaphragm-through joints. Analytical methods proposed by Sasaki *et al.* (1995), Lu *et al.* (2000) and Nie *et al.* (2009) provide useful tools for the study of diaphragm-through joints. All of these analytical methods compute the flexural bearing capacity of the panel zone of joints as the tension force transferred from steel beam flange multiplied by the central distance between two diaphragms, as shown in Fig. 2(a). The tension force is evaluated based on two assumed yielding mechanisms of the steel tube and the diaphragm according to yield line theory, shown in Figs. 2(b)-(c). In Fig. 2, P is the tensile capacity of the panel zone, M is the flexural bearing capacity of the panel zone, h is the distance between the beam flanges, P_c is the tensile capacity of the steel tube and P_d is the tensile capacity of the diaphragm.

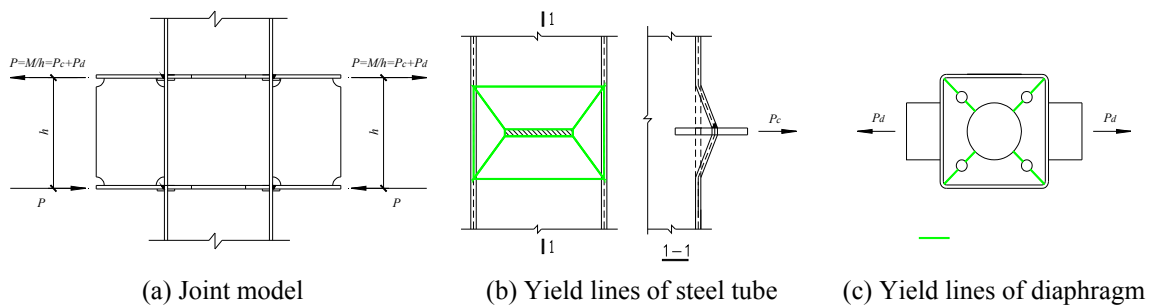


Fig. 2 Yield lines of diaphragm

Table 2 Material properties of steel

Component	Thickness (mm)	f_y (N/mm ²)	f_u (N/mm ²)	E_s (10 ⁵ N/mm ²)	δ (%)
Tube	8	284.7	409.8	2.036	33.6
	10	316.1	463.3	2.180	38.7
Plate	8	279.7	459.7	1.887	39.6
	10	302.8	421.4	1.952	37.4
	12	305.2	429.8	2.167	34.6

Table 3 Material properties of concrete

Cement (kg/m ³)	Sand (kg/m ³)	Coarse aggregate (kg/m ³)	f_c (N/mm ²)	E_c (10 ⁴ N/mm ²)
460	720	1036	47.6	3.73

these specimens, the steel beam and the diaphragm have the same thickness and all steel webs are 8 mm in thickness.

The specimens were manufactured from cold-formed square steel tubes as well as diaphragms and beams made from steel plates. The tubes were connected with the diaphragm with butt weld. Before concrete casting, a square steel base plate was welded at the bottom of each specimen. The concrete was cured for 28 days.

2.2 Material properties

Tension coupons were cut from steel tubes and steel plates and they were tested to determine the material properties of the steel. The yield strength f_y , the ultimate strength f_u , the modulus of elasticity E_s and the elongation ratio δ are listed in Table 2.

Concrete cubes were cast and cured in the same conditions same to those of the experiment and tested in compression. The mixture of the concrete, as well as the measured average crushing strength f_c and the module of elasticity E_c are listed in Table 3.



Fig. 4 Loading set-up

2.3 Loading and measurement

Fig. 4 gives a general view of the static tensile loading test set-up. A 1000 kN capacity axial tensile testing machine is used to stretch the specimen by clamping flanges. A load increment of about 1/10 of the estimated maximum loading was applied. Each load interval was maintained for about 10 minutes. The load-displacement curve was recorded continuously during the loading. When the slope of the load-displacement curve starts to change, it was assumed that the specimen entered the yield stage and the load increment was decreased to about 1/25 of the estimated maximum loading until failure.

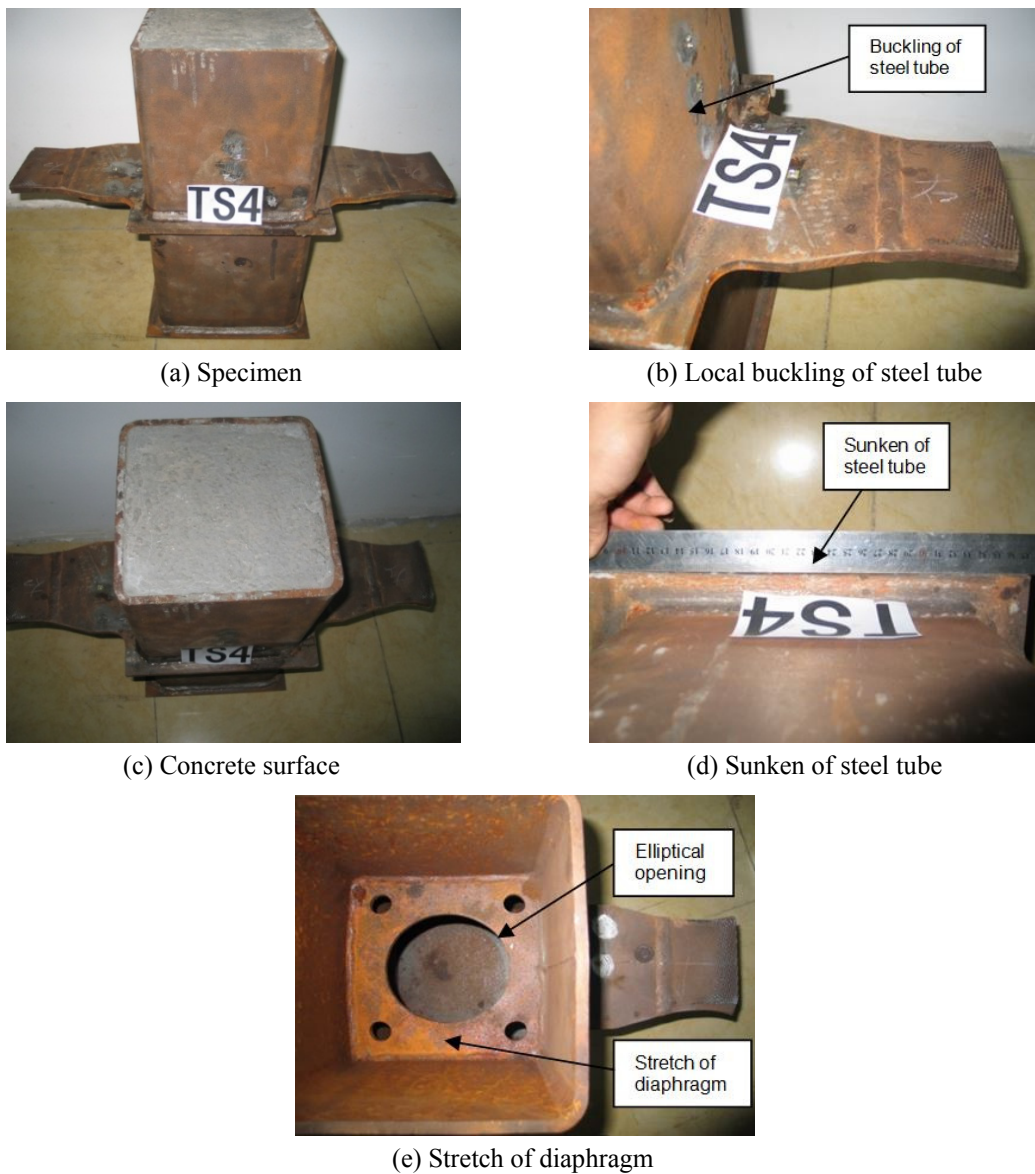


Fig. 5 Failure modes

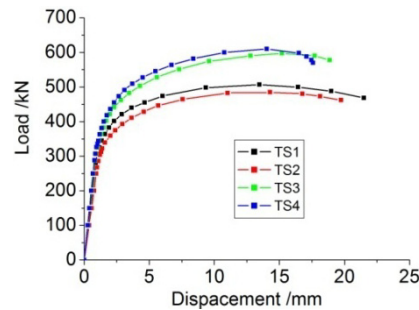


Fig. 6 Load-displacement curves

Table 4 Bearing capacity of specimens

Specimen	P_y^e (kN)	P_u^e (kN)	P_u^b (kN)
TS1	363.6	507.2	526.8
TS2	339.3	484.8	526.8
TS3	402.1	597.7	644.7
TS4	418.3	610.2	644.7

2.4 Test results and discussion

2.4.1 Failure modes

The failure mode of all the tested specimens is similar: failure of the panel zone. Fig. 5 shows the typical failure mode. During the early stage of loading, no cracks were observed on concrete surface and there were no obvious deformations in the specimen. When the load reached about 60%-70% of the failure load, excessive stretch of the diaphragm and signs of local buckling of the steel tube appeared gradually leading to failure as shown in Fig. 5(b). At the failure load, the deformation of diaphragm and the local buckling were obvious and the specimen cannot take any more loading, while there were still no cracks found on the surface of concrete as shown in Fig. 5(c). After the removal of the in-filled concrete, it was found that the circular openings of the diaphragm were stretched to ellipse as shown in Fig. 5(e).

2.4.2 Load-displacement curves

Fig. 6 shows the load-displacement curve of the specimens. It is found that all the test specimens behave in a relatively ductile manner and testing is proceeded in a smooth and controlled fashion. All curves exhibit elastic behavior at the initial stage followed by a clear extensive plastic plateau indicating good ductility.

The yield load P_y^e and the failure load P_u^e which are obtained from the load-displacement curve of each specimen are listed in Table 4. A graphical method (Nie *et al.* 2008b) is employed to catch the yield load P_y^e . In Table 4, the ultimate load of the beam flange P_u^b which is calculated by $P_u^b = f_u \cdot t_f \cdot b_f$ is also listed. In this expression, f_u is the ultimate strength, t_f is the thickness and b_f is the width of the flange.

2.4.3 Discussions

From Table 4, it can be seen that the failure load of each specimen is less than the ultimate load

of beam flange. Considering the obvious deformation in the diaphragm and the buckling of steel tube at the failure point of the specimens, shown in Fig. 5, it is apparent that the failure mode of these specimens is the failure of the panel zone of the joint.

From Fig. 6 and Table 4, it is apparent that the smaller diameter of the central opening in the diaphragm is beneficiary leading to larger failure load. Note that in specimens TS1 and TS2 the only difference is the diameter of the opening that changes from 140 mm to 160 mm. The effect of the thickness of the diaphragm is demonstrated in specimens TS2 and TS3 in which the thickness is the only one parameter that changes from 10 mm to 12 mm. It is found that the larger thickness of diaphragm in panel zone remarkably increases the failure load. Finally the effect of the thickness of steel tube is demonstrated in specimens TS3 and TS4 in which the thickness of steel tube is the only parameter that changes from 8 mm to 10 mm. It indicates that increasing the thickness of steel tube can enlarge the failure load of panel zone of diaphragm-through joint.

3. Finite element analysis

In order to compare the experimental results with analytical predictions, a nonlinear finite element analysis has been undertaken using the finite element package ANSYS 12.0. The three-dimensional finite element models have the same size and material properties with the specimens of the static tensile loading experiments described before.

3.1 Finite element model

3.1.1 Steel members modeling

The three-dimensional 20-node element SOLID 95 is adopted to model the steel tube, the diaphragm, the beam flange and the beam web. Each node of the element has three translation degrees of freedom. This element is capable to capture plasticity, large deflections, and large strains.

The tri-linear stress-strain relation proposed by Nie *et al.* (2008a) is used to model the constitutive law of the steel members as shown in Fig. 7, where $\epsilon_y = f_y / E_s$, $\epsilon_u = 10(f_u - f_y) / E_s$. The values of the yield strength f_y , the ultimate strength f_u and the modulus of elasticity E_s are the values found in the static tensile loading test. The Poisson's ratio of the steel members is assumed as 0.3.

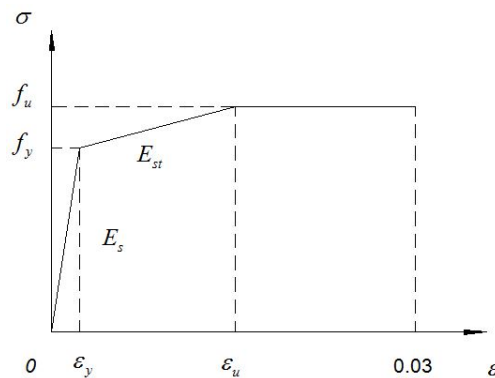


Fig. 7 Constitutive law of steel members

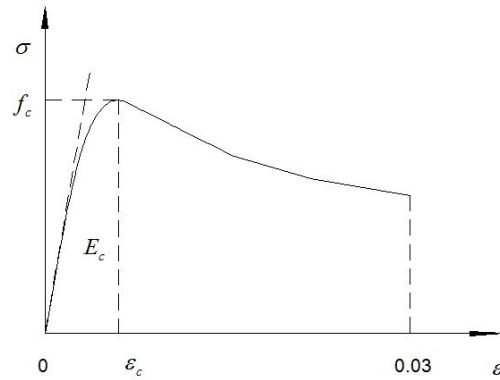


Fig. 8 Constitutive law of concrete

3.1.2 Concrete modeling

The three-dimensional 8-node element SOLID 65 is used to model the in-filled concrete. Each node of the element has three translation degrees of freedom. This element is capable of capturing the effects of cracking in tension, crushing in compression, and plastic deformation.

The constitutive law of concrete proposed by Li and Han (2011, 2012) is used for the in-filled concrete as shown in Fig.8. The values of the compressive strength σ_c and the modulus of elasticity E_c of the concrete are the values found in the static test. The Poisson's ratio of the in-filled concrete is assumed equal to 0.2.

3.1.3 Modeling of the concrete-steel interface

The contact elements TARGET 170 and CONTA 174 are employed to model the contact action between the steel members and the concrete. These contact elements allow the surfaces to separate under tensile force but not penetrate each other. The friction between two faces is maintained as long as the surfaces remain in contact. The coefficient of friction between the two faces is taken as 0.25 in the analysis.

3.1.4 Modeling of loading and boundary conditions

The tensile load is transferred through the flange of the steel beam acting on both sides of the diaphragm. To simulate this action one side of the beam flange is fixed and the tensile load is

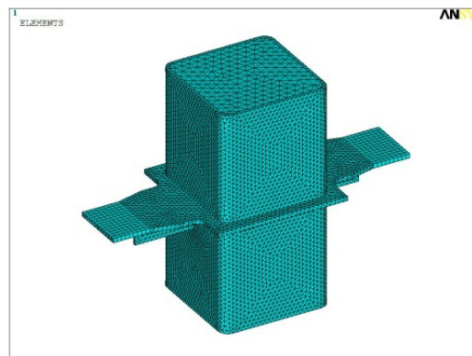


Fig. 9 Finite element joint

applied on the other end. The loads are applied as static uniform load using displacement control at each node of the loaded surfaces, and the displacement increments are identical to the increments of the static tensile loading test. The finite element models are shown in Fig. 9.

3.2 Verifications

3.2.1 Failure modes and load transfer mechanism

The predicted failure modes of all specimens are similar. A typical predicted failure mode and stress contours of specimen TS2 are shown in Fig. 10. The numerical results indicate that at the failure point, the diaphragm and the nearby steel tube reach the ultimate strength while the stress levels of the concrete core and the beam webs are lower than the ultimate strength as shown in Figs. 10(a)-(b). Moderate buckling occurs on the steel tube and the diaphragm is stretched with the central opening deformed from circle to ellipse as shown in Figs. 10(c)-(d). The predicted failure mode demonstrates that failure is caused by overstress of the diaphragm and the steel tube at the panel zone of the joint. These numerical results are in good agreement with the static tensile test results.

The finite element analysis and the static tensile loading experiment show that, as the load increases, the load is transferred to the steel tube, the diaphragm and the concrete core. From Fig.

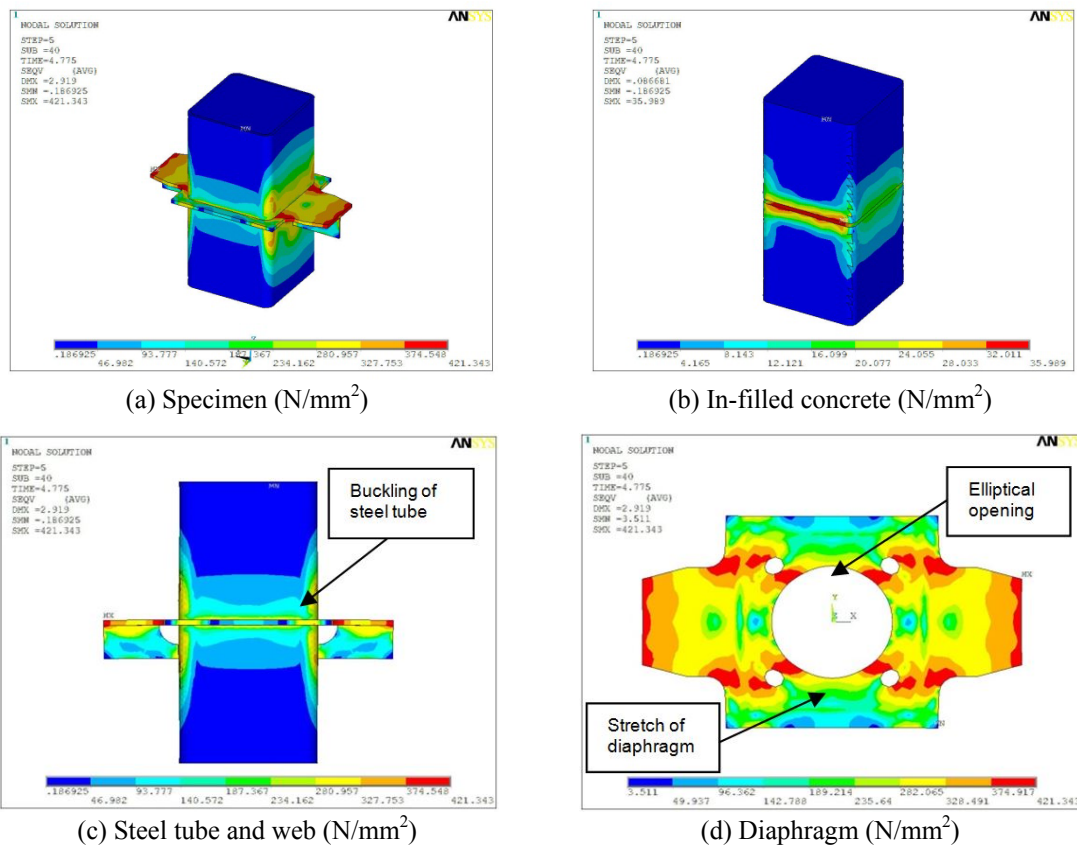


Fig. 10 Failure mode and stress contour of specimen TS2

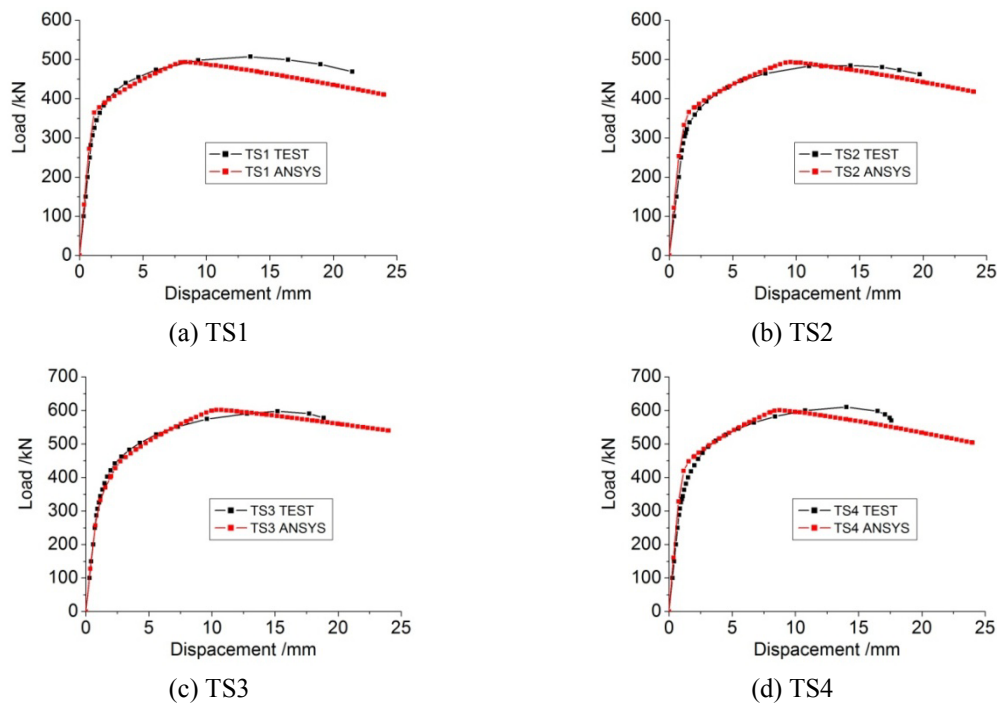


Fig. 11 Comparison of load-displacement curves

10, it can be seen that there is a large stress distribution zone in the diaphragm and the nearby steel tube while the stress level of the concrete is lower with a smaller distribution zone. It shows that the tensile load from the steel beam flange is mainly transfer to the steel tube and the diaphragm.

3.2.2 Load-displacement curves

The load-displacement curves obtained by the finite element analysis are compared with the test curves in Fig. 11. The predicted load-displacement curves of all specimen have a linear elastic behavior at the initial stage followed by inelastic behavior when the load is further increased. All load-displacement curves are in good agreement with the experimental ones.

The yield loads P_y^f and the ultimate loads P_u^f obtained from the predicted curves by using graphical method (Nie *et al.* 2008b) are listed in Table 5 and they are compared with the experimental ones. The analytical values are in good agreement with the experimental ones.

Table 5 Comparison of bearing capacity

Specimen	Yield bearing capacity			Ultimate bearing capacity		
	P_y^e (kN)	P_y^f (kN)	P_y^f / P_y^e	P_u^e (kN)	P_u^f (kN)	P_u^f / P_u^e
TS1	363.6	377.8	1.04	507.2	493.6	0.97
TS2	339.3	366.2	1.08	484.8	491.9	1.01
TS3	402.1	384.7	0.96	597.7	601.5	1.01
TS4	418.3	448.1	1.07	610.2	607.1	0.99

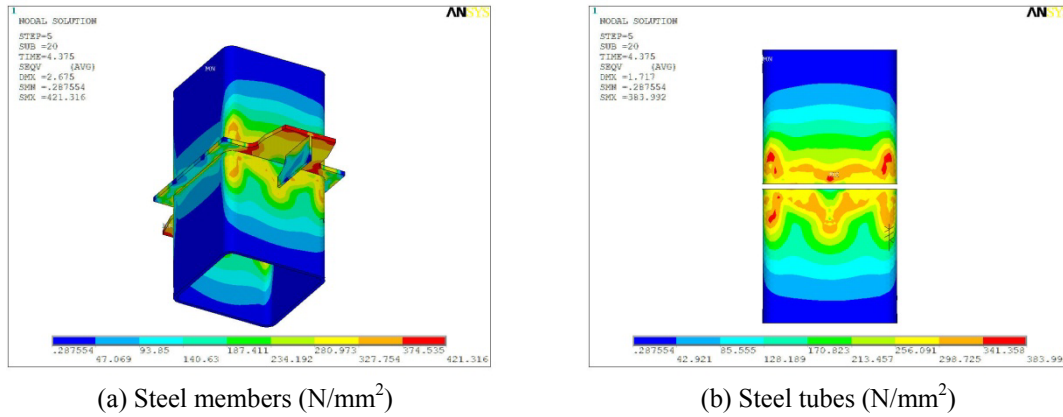


Fig. 12 Von Mises stress in steel tube

4. Theoretical analysis

The overall agreement between the experimental and the numerical results demonstrates the feasibility and accuracy of the finite element analysis. According to results of experiments and finite element analysis, the analytical method for calculation of bearing capacity of these specimens is studied based on yield line theory.

4.1 The yield mechanism of the steel tube

Fig. 12 shows the typical distribution of the plastic zone in the steel tube as obtained from the finite element analysis. The stress level of the steel tube is higher along the loading direction with a larger distribution area, while in the perpendicular direction the stress level is lower with a smaller distribution area. The plastic zone appears mainly in the intersection of the steel tube and the diaphragm. The beam web causes a different distribution of plastic zone between the upper and the lower steel tube.

The plastic zone in the steel tubes as shown in Fig. 12(b) does not compare well with the yield line model of the steel tube proposed in previous research works as it is shown in Fig. 2(b). Fig. 12(b) shows that the distribution of plastic zone in the lower steel tube with steel beam web is different with the distribution of plastic zone in the upper steel tube. It proves that the influence of steel beam web which has a constraint action on steel tube should be considered in the yield lines pattern of steel tube.

Based on the distribution of the plastic zone of Fig. 12, the yield line model of Fig. 13 is more realistic considering the influence of the beam web and the joint configuration.

According to the calculation method of the stepped yield line (Lee *et al.* 2012, Qin *et al.* 2014), the yield tensile capacity of the steel tube P_c^y can be expressed as

$$P_c^y = \left(\frac{D+Y-t_c}{X} + \frac{2X+3h_w}{Y} + \frac{D+Y-t_c}{h_w} \right) \frac{f_{yc}t_c^2}{2} \quad (1)$$

Where, D is the width of steel tube, t_c is the thickness of steel tube, b_f is the width of beam flange, h_w is the height of beam web as shown in Fig. 3 and f_{yc} is the yield strength of the steel tube.

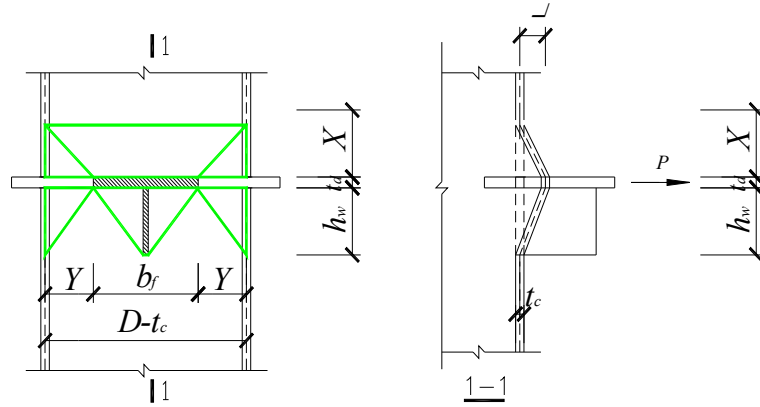
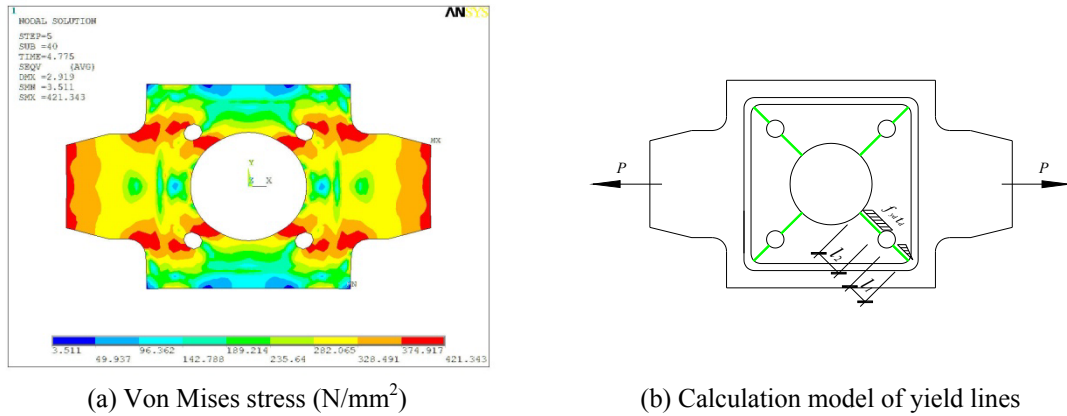


Fig. 13 Calculation model of yield lines in steel tube



(a) Von Mises stress (N/mm²)

(b) Calculation model of yield lines

Fig. 14 Calculation model of yield lines in diaphragm

The distance X is calculated as $X = \sqrt{(D + Y - t_c)Y/2}$ which is determined by the principle of virtual work ($\partial P_c^y / \partial X = 0$). The distance Y is calculated as $Y = (D - t_c - b_f) / 2$.

4.2 The yield mechanism of the diaphragm

Fig. 14(a) shows the typical distribution of plastic zone of the diaphragm as obtained from the finite element analysis. The stress contour shows that the stress levels are larger along the loading direction. In the perpendicular direction they are smaller, especially in the cantilevered section. It seems that the tensile load from the flange is mainly transferred to the section of the diaphragm enclosed by the steel tube and a plastic zone appears along the diagonals of the cross-section lines enclosed by the tube.

Based on the stress contour, the yielding will take place along the diagonals of the diaphragm which is similar to the yield mechanism of interior diaphragm joints shown in Fig. 2(c). Therefore, the yielding mechanism of the diaphragm is similar to the yield mechanism of interior diaphragm joints (Nie *et al.* 2009) and it is shown in Fig. 14(b). The yield tensile capacity of diaphragm P_d^y can be calculated as

Table 6 Comparison of bearing capacity

Specimen	Yield bearing capacity			Ultimate bearing capacity		
	P_y^e (kN)	P_y (kN)	P_y / P_y^e	P_u^e (kN)	P_u (kN)	P_u / P_u^e
TS1	363.6	345.1	0.95	507.2	486.8	0.96
TS2	339.3	303.9	0.90	484.8	429.5	0.89
TS3	402.1	387.4	0.96	597.7	549.9	0.92
TS4	418.3	412.4	0.99	610.2	593.2	0.97

$$P_d^y = \sqrt{2}t_d f_{yd} (l_2 + l_1 / 2) \tag{2}$$

Where, t_d is the thickness of the diaphragm, f_{yd} is the yield stress of the diaphragm and l_1 and l_2 are the lengths of yield lines.

4.3 Verification of the analytical method

In order to validate the accuracy of the analytical method proposed above, the experimental yield and ultimate bearing capacity of static tensile loading tests are compared with the calculated ones. The total ultimate bearing capacity of the specimens P_u , can be calculated by using equations (1) and (2) if the yield strength is substituted by the ultimate

$$P_u = \left(\frac{D+Y-t_c}{X} + \frac{2X+3h_w}{Y} + \frac{D+Y-t_c}{h_w} \right) \frac{f_{yc}t_c^2}{2} + \sqrt{2}t_d f_{ud} (l_2 + l_1 / 2) \tag{3}$$

Where, f_{uc} is the ultimate strength of steel tube and f_{ud} is the ultimate stress of the diaphragm.

Comparisons of the experimental and theoretical values for yield and ultimate bearing capacity shown in Table 6, indicates a good agreement.

5. Conclusions

Static tensile loading experiments and nonlinear finite element analysis have shown that for diaphragm-through joints with a failure of panel zone, the tensile load from the steel beam flange is mainly shared by the square steel tube and the diaphragm.

According to the finite element analysis which is in a good agreement with the test results, the diaphragm plastic zone appears along the cross-section lines enclosed by the square steel tube and the influence of the beam web on the plastic zone of steel tube is significant and cannot be neglected.

An improved yield line model is proposed which takes into account the influence of the beam web. Base on this yield line model, an analytical method for the computation of the tensile bearing capacity of the joint is proposed. The computed capacities are in good agreement with the experimentally obtained.

Acknowledgments

The research described in this paper was financially supported by the National Natural Science

Foundations of China (No. 51268054 and No. 51468061) and the Natural Science Foundation of Tianjin City, China (No. 13JCQNJC07300). The financial supports are greatly appreciated.

References

- Choi, S., Lee, S., Hong, S. and Kim, J. (2009), "Structural capacities of tension side for CFT square column-to-beam connections with combined-cross diaphragm", *Adv. Struct. Eng.*, **11**(2), 209-227.
- Han, L.H. and Li, W. (2010), "Seismic performance of CFST column to steel beam joint with RC slab: experiments", *J. Constr. Steel Res.*, **66**(11), 1374-1386.
- Kim, T., Stojadinovic, B. and Whittaker, A.S. (2008), "Seismic performance of pre-northridge welded steel moment connections to built-up box columns", *J. Struct. Eng.*, **134**(2), 289-299.
- Lee, S.H., Kim, Y.H. and Choi, S.M. (2012), "Shear strength formula of CFST column-beam pinned connections", *Steel Compos. Struct., Int. J.*, **13**(5), 409-421.
- Li, W. and Han, L.H. (2011), "Seismic performance of CFST column to steel beam joint with RC slab: Analysis", *J. Constr. Steel Res.*, **67**(1), 127-139.
- Li, W. and Han, L.H. (2012), "Seismic performance of CFST column to steel beam joint with RC slab: Joint model", *J. Struct. Eng.*, **73**(6), 66-79.
- Liu, Y., Malaga-Chuquitaype, C. and Elghazouli, A.Y. (2012), "Behaviour of beam-to-tubular column angle connections under shear loads", *Eng. Struct.*, **42**(9), 434-456.
- Lu, X.L., Yu, Y., Kiyoshi, T. and Satoshi, S. (2000), "Experimental study on the seismic behavior in the connection between CFRT column and steel beam", *Struct. Eng. Mech., Int. J.*, **9**(4), 365-374.
- Nie, J.G., Qin, K. and Cai, C.S. (2008a), "Seismic behavior of connections composed of CFSSTCs and steel-concrete composite beams- finite element analysis", *J. Constr. Steel Res.*, **64**(6), 680-688.
- Nie, J.G., Qin, K. and Cai, C.S. (2008b), "Seismic behavior of connections composed of CFSSTCs and steel-concrete composite beams-experimental study", *J. Constr. Steel Res.*, **64**(10), 1178-1191.
- Nie, J.G., Qin, K. and Cai, C.S. (2009), "Seismic behavior of composite connections-flexural capacity analysis". *J. Constr. Steel Res.*, **65**(5), 1112-1120.
- Qin, Y., Chen Z. and Wang, X. (2014), "Elastoplastic behavior of through-diaphragm connections to concrete-filled rectangular steel tubular columns", *J. Constr. Steel Res.*, **93**(2), 88-96.
- Sasaki, S., Teraoka, M., Morita, K. and Fujiwara, T. (1995), "Structural behavior of concrete-filled square tubular column with partial-penetration weld corner seam to steel H-beam connections", *Proceedings of the 4th Pacific Structural Steel Conference*, Pergamon, UK, pp. 33-40.
- Tizani, W., Wang, Z.Y. and Hajirasouliha, I. (2013), "Hysteretic performance of a new blind bolted connection to concrete filled columns under cyclic loading: An experimental investigation", *Eng. Struct.*, **46**(1), 535-546.
- Wang, J.F., Chen, X. and Shen, J. (2012), "Performance of CFTST column to steel beam joints with blind bolts under cyclic loading", *Thin Wall. Struct.*, **60**(12), 69-84.
- Zhao, X.L., Han, L.H. and Lu, H. (2010), *Concrete-filled Tubular Members and Connections*, Taylor & Francis, Abingdon, OX, UK.